J. Fluid Mech. (1972), *vol.* 56, *part* 4, *pp.* 629–639
Printed in Great Britain

Viscous effects in a vertically propagating internal wave

By D. GORDON AND T. N. STEVENSON
Department of the Mechanics of Fluids, University of Manchester

(Received 26 July 1972)

A circular cylinder is positioned horizontally in an incompressible stably stratified fluid which has a constant Brunt–Väisälä frequency. A vertical two-dimensional internal wave is produced when the cylinder is oscillated at this natural frequency. A small amplitude viscous similarity solution which explains the main features of the internal wave is presented.

1. Introduction

Small amplitude inviscid theory for internal waves in stably stratified fluids (Görtler 1943; Mowbray & Rarity 1967) shows that the phase velocity, which is normal to the group velocity, is directed away from the vertical and shows that the group velocity vector approaches the vertical and decreases to zero magnitude as the forcing frequency increases towards the natural frequency of the fluid. In this paper experiments are described in which a horizontal cylinder, in a stably stratified salt solution with constant natural frequency, is oscillated at this frequency. A narrow vertical two-dimensional internal wave is produced, and the phase velocities, which are directed away from the vertical, together with the fluid displacements within the wave are measured.

A small amplitude viscous similarity analysis is shown to compare quite well with the main features of the experiment providing that the reflexions from the upper and lower surfaces of the working tank are taken into account. The analysis is similar to that used by Thomas & Stevenson (1972) for the viscous internal cross-wave.

2. Analysis

A horizontal two-dimensional body oscillates with frequency ω in an unbounded, incompressible, density stratified, non-diffusive fluid. A Cartesian co-ordinate system $Ox'y'$ is chosen which is stationary relative to the undisturbed fluid with x' measured vertically upwards and y' measured horizontally, normal to the longitudinal axis of the cylinder (see figure 1, plate 1). The mean position of the body is on the x' axis. An exponential distribution of the background density $\rho_0 = \rho^* \exp(-\beta x')$ implies a constant Brunt–Väisälä frequency $\omega = (g\beta)^{\frac{1}{2}}$, where g is the acceleration due to gravity and ρ^* and β are constants. The velocity components in the x' and y' directions are u' and v' respectively, the density is ρ_T, μ_T is the viscosity, p_T is the pressure and t' is the time. The perturbation variables $p' = p_T - p_0$, $\rho' = \rho_T - \rho_0$ and $\mu' = \mu_T - \mu_0$ are introduced, μ_0 and p_0

being the background equilibrium values. The equations of continuity and incompressibility are

$$\frac{\partial u'}{\partial x'}+\frac{\partial v'}{\partial y'}=0, \tag{1}$$

$$\frac{\partial \rho'}{\partial t'}+u'\frac{\partial \rho_T}{\partial x'}+v'\frac{\partial \rho'}{\partial y'}=0 \tag{2}$$

and the perturbation momentum equations obtained by subtracting the hydrostatic relations are

$$\rho_T\left(\frac{\partial u'}{\partial t'}+u'\frac{\partial u'}{\partial x'}+v'\frac{\partial u'}{\partial y'}\right)=-\frac{\partial p'}{\partial x'}+2\frac{\partial}{\partial x'}\left(\mu_T\frac{\partial u'}{\partial x'}\right)+\frac{\partial}{\partial y'}\left[\mu_T\left(\frac{\partial u'}{\partial y'}+\frac{\partial v'}{\partial x'}\right)\right]-\rho' g \tag{3}$$

and

$$\rho_T\left(\frac{\partial v'}{\partial t'}+u'\frac{\partial v'}{\partial x'}+v'\frac{\partial v'}{\partial y'}\right)=-\frac{\partial p'}{\partial y'}+2\frac{\partial}{\partial y'}\left(\mu_T\frac{\partial v'}{\partial y'}\right)+\frac{\partial}{\partial x'}\left[\mu_T\left(\frac{\partial u'}{\partial y'}+\frac{\partial v'}{\partial x'}\right)\right]. \tag{4}$$

The boundary conditions are that u', v', p', ρ' and their derivatives tend to zero as $y' \to \pm\infty$.

The variables are made dimensionless as follows:

$$t'=t\omega^{-1},\quad x'=x\beta^{-1},\quad y'=y\alpha\beta^{-1},\quad \rho'=\rho a\rho^*,$$

$$u'=uag\omega^{-1},\quad v'=v\alpha ag\omega^{-1},\quad \mu'=\mu a\mu^*,\quad p'=p\alpha^2 ag\rho^*\beta^{-1},$$

where $\alpha=(\omega^3\nu^*2/g^2)^{\frac{1}{4}}$, $\nu^*=\mu^*/\rho^*$, μ^* is a constant reference viscosity and a is a constant amplitude coefficient.

The experiments which are described in the next section show that the internal wave is confined to a narrow region close to the x' axis and that the particle oscillations are virtually along lines parallel to this axis. In the analysis we assume that the velocity in the y' direction is small compared with that in the x' direction such that $\alpha \ll 1$.

Equations (1)–(4) reduce to

$$\partial u/\partial x+\partial v/\partial y=0, \tag{5}$$

$$\partial \rho/\partial t=ur_0+O(a), \tag{6}$$

$$r_0\left(\frac{\partial u}{\partial t}\right)=-\rho-\alpha^2\left(\frac{\partial p}{\partial x}-\frac{\gamma_0}{2}\frac{\partial^2 u}{\partial y^2}\right)+O(a)+O(\alpha^4) \tag{7}$$

and

$$r_0\left(\frac{\partial v}{\partial t}\right)=-\frac{\partial p}{\partial y}+\frac{\alpha^2\gamma_0}{2}\frac{\partial^2 v}{\partial y^2}+\frac{\alpha^2}{2}\frac{\partial \gamma_0}{\partial x}\frac{\partial u}{\partial y}+O(a)+O(\alpha^4), \tag{8}$$

where $r_0=\rho_0/\rho^*=\exp(-x)$ and $\gamma_0=\mu_0/\mu^*$.

With the assumption that $a \ll \alpha^2$ the dependent variables are expanded as

$$u=u_1+\alpha^2 u_2+\ldots,\quad v=v_1+\alpha^2 v_2\ldots,$$

$$\rho=\rho_1+\alpha^2\rho_2\ldots,\quad p=p_1+\alpha^2 p_2\ldots .$$

These are now substituted into (6)–(8) and terms of like order in α^2 are equated. In the resulting linear system, a time dependence factor e^{-it} is assumed and the equations reduce to

$$ir_0 u_1 = \rho_1, \tag{9}$$

$$-i\rho_2 = u_2 r_0, \tag{10}$$

$$ir_0 v_1 = \partial p_1/\partial y, \tag{11}$$

$$ir_0 u_2 = \frac{\partial p_1}{\partial x} + \rho_2 - \frac{\gamma_0}{2}\frac{\partial^2 u_1}{\partial y^2} \tag{12}$$

and

$$ir_0 v_2 = \frac{\partial p_2}{\partial y} - \frac{\gamma_0}{2}\frac{\partial^2 v_1}{\partial y^2} - \frac{1}{2}\frac{\partial \gamma_0}{\partial x}\frac{\partial u_1}{\partial y}. \tag{13}$$

The continuity equation allows us to introduce the stream function $\psi(x, y)$ defined by $u_1 = \partial\psi/\partial y$ and $v_1 = -\partial\psi/\partial x$ with $\psi(x, \infty) = 0$.

ρ_2 and u_2 are eliminated between (10) and (12) to give

$$\frac{\gamma_0}{2}\frac{\partial^3 \psi}{\partial y^3} = \frac{\partial p_1}{\partial x} \tag{14}$$

and (11) is written as

$$-ir_0 \frac{\partial \psi}{\partial x} = \frac{\partial p_1}{\partial y}. \tag{15}$$

From these equations it is evident that either p_1 is an even function of y and ψ an odd function, or vice versa.

The momentum flux condition is obtained by integrating (14) across the wave to yield

$$\int_{-\infty}^{\infty} p_1 \, dy = J. \tag{16}$$

The constant J is assumed to be non-zero and so p_1 is taken to be an even function of y. A solution is sought in the interval $0 \leqslant y < +\infty$, and may be continued into the interval $-\infty < y \leqslant 0$ by using

$$p_1(x, -y) = p_1(x, y) \quad \text{and} \quad \psi(x, -y) = -\psi(x, y).$$

An integral condition on ψ is obtained by multiplying (15) by y and integrating across the wave:

$$\int_0^{\infty} y\psi \, dy = -\tfrac{1}{2} iJ(e^x + c), \tag{17}$$

where c is a constant.

Equations (14) and (15) subject to the integral constraints (16) and (17) may be written as ordinary differential equations in the transformed co-ordinate system (x, η), where

$$\eta = y(e^x + c)^{1/(2m-2)},$$

providing

$$\gamma_0 = r_0^{(m+1)/(m-1)}(1 + cr_0)^{2m/(1-m)} = e^x(e^x + c)^{2m/(1-m)},$$

$p_1 = (e^x + c)^{1/(2-2m)} P(\eta)$, $\psi = (e^x + c)^{m/(m-1)} F(\eta)$, where m is a constant; $m \neq 1$. Equations (14) and (15) become

$$P + \dot{P}\eta = (m-1)\ddot{F} \tag{18}$$

and

$$2i(m-1)\dot{P} = 2mF + \eta\dot{F}. \tag{19}$$

Using the conditions as $\eta \to \infty$, equation (18) integrates to

$$P = (m-1)\ddot{F}/\eta, \tag{20}$$

which is substituted into (19) to give

$$2i(m-1)^2 \frac{d}{d\eta}\left(\frac{\dot{F}_m}{\eta}\right) = 2mF_m + \eta \dot{F}_m. \tag{21}$$

The subscript refers to the value of the parameter m. The integral condition (17) becomes

$$\int_0^\infty \eta F_m \, d\eta = -\tfrac{1}{2} i J_m. \tag{22}$$

Equation (21) is solved for F_m subject to condition (22) and the boundary conditions as $\eta \to \infty$. Analytic solutions exist for positive even integer values of the parameter m. The solutions for $m = 0$ and 2 are

$$F_0 = -i(1-i)^{\frac{3}{2}} \frac{J_0}{2\sqrt{\pi}} \int_\eta^\infty \exp\left[-\tfrac{1}{4}(1-i)\,k^2\right] dk \tag{23}$$

and

$$F_2 = -i(1-i)^{\frac{3}{2}} \frac{J_2}{4\sqrt{\pi}} \eta \exp\left[-\tfrac{1}{4}(1-i)\,\eta^2\right].$$

For $m \geqslant 2$ the solutions are of the form

$$F_m = \eta K_{\frac{1}{2}(m-2)}(\eta^2) \exp\left[-\{(1-i)/\lambda_m\}/\eta^2\right],$$

where λ_m is a positive real constant and $K_r(z)$ is a complex polynomial in z of order r.

For $m = 4$ the solution is

$$F_4 = (1-i)^{\frac{1}{2}} \frac{J_4}{72(3\pi)^{\frac{1}{2}}} \left[\eta^3 - 15(1+i)\,\eta\right] \exp\left[-\tfrac{1}{12}(1-i)\,\eta^2\right].$$

The important dependent variables are found from

$$u_{1m} = (e^x + c)^{(2m+1)/2(m-1)} \dot{F}_m,$$

$$v_{1m} = -\left[1/2(m-1)\right] e^x (e^x + c)^{1/(m-1)} (\eta \dot{F}_m + 2mF_m),$$

$$\rho_{1m} = i\, e^{-x} (e^x + c)^{(2m+1)/2(m-1)} \dot{F}_m$$

and

$$p_{1m} = (m-1)\,(e^x + c)^{1/(2m-2)} \ddot{F}_m/\eta.$$

In this paper we are primarily interested in an internal wave solution which originates from a small forcing region near the origin so that, at fixed η, $y \to 0$ as $x \to 0$. This condition, together with the conditions $r_0 = \gamma_0 = 1$ at $x = 0$, is compatible with the $m = 0$ similarity solution providing that $c = -1$. If F_0 is written as

$$F_0 = -A \int_\eta^\infty \exp\left[-\tfrac{1}{4}(1-i)\,k^2\right] dk$$

the dependent variables are

$$u_1 = A(e^x - 1)^{-\frac{1}{2}} \exp\left[\tfrac{1}{4}(i-1)\,\eta^2\right],$$

$$v_1 = \tfrac{1}{2} A\, e^x (e^x - 1)^{-1} \eta \exp\left[\tfrac{1}{4}(i-1)\,\eta^2\right],$$

$$\rho_1 = iA\, e^{-x} (e^x - 1)^{-\frac{1}{2}} \exp\left[\tfrac{1}{4}(i-1)\,\eta^2\right]$$

and

$$p_1 = \tfrac{1}{2}(1-i)\, A(e^x - 1)^{-\frac{1}{2}} \exp\left[\tfrac{1}{4}(i-1)\,\eta^2\right].$$

The implied relation between r_0 and γ_0 is $r_0 = \gamma_0^{-1}$ and $\eta = y(e^x - 1)^{-\frac{1}{2}}$.

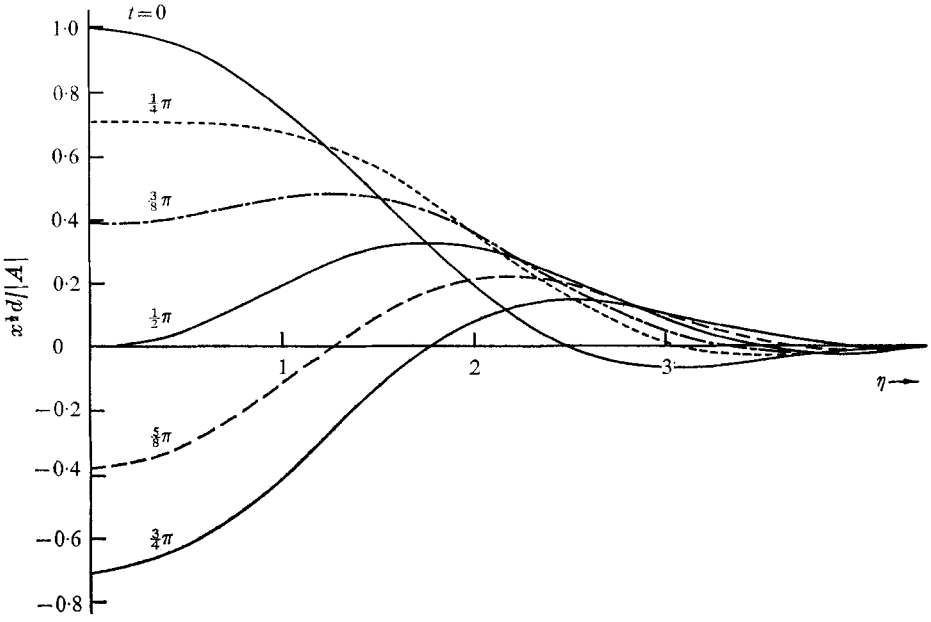

FIGURE 2. Displacement profiles during a half cycle evaluated from (26).

If the Boussinesq approximation had been made initially then the solution would be the same as the small x version of the above relations. In this case, with the time dependency included and the real parts evaluated, we have

$$u_1 = |A|\, x^{-\frac{1}{2}} \cos(\tfrac{1}{4}\eta^2 - t + \arg A) \exp(-\tfrac{1}{4}\eta^2), \tag{24}$$

$$v_1 = \tfrac{1}{2}|A|\, x^{-1}\eta \cos(\tfrac{1}{4}\eta^2 - t + \arg A) \exp(-\tfrac{1}{4}\eta^2), \tag{25}$$

$$\rho_1 = |A|\, x^{-\frac{1}{2}} \cos(\tfrac{1}{4}\eta^2 - t + \arg A + \tfrac{1}{2}\pi) \exp(-\tfrac{1}{4}\eta^2), \tag{26}$$

$$p_1 = (|A|/\sqrt{2})\, x^{-\frac{1}{2}} \cos(\tfrac{1}{4}\eta^2 - t + \arg A - \tfrac{1}{4}\pi) \exp(-\tfrac{1}{4}\eta^2), \tag{27}$$

and the particle displacement d from the undisturbed position is equal to ρ_1. In these simplified equations $\eta = y/x^{\frac{1}{2}}$.

The phase lag t_p relative to the phase along $\eta = 0$ is given by $t_p = \frac{1}{4}\eta^2$. The phase velocity is therefore directed away from the vertical axis and decreases as η increases.

The solution to the Boussinesq equations is symmetrical about $x = 0$ and therefore (24)–(27) may be applied to the wave propagating downwards providing that x is measured positively downwards.

In figure 2 a few displacement profiles during a half cycle show how the crests move outwards with time. The u and v velocities, the displacement and the perturbation pressure are shown at two time instants in figure 3.

3. Experiments

A glass-sided tank 1·8 m long, 0·9 m high and 0·55 m from front to back was filled with stratified brine which had an almost constant Brunt–Väisälä frequency of 1·12 rad s^{-1}. A horizontal circular cylinder was connected by a vertical strut

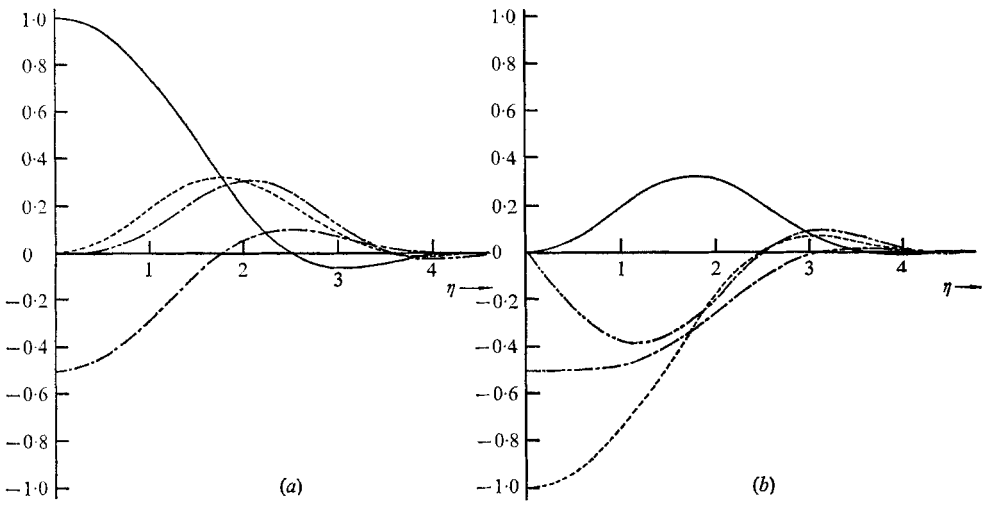

FIGURE 3. The u and v velocity distributions, the displacement profile and the pressure distribution evaluated from (24) to (27) at two instants of time $\pi/2\omega$ apart. (*a*) $t = 0$. (*b*) $t = \frac{1}{2}\pi$. – – –, $u_1 x^{\frac{1}{2}}/|A|$; — · · — · ·, $v_1 x/|A|$; ——, $x^{\frac{1}{2}}d/|A|$; — · — ·, $p_1 x^{\frac{1}{2}}/|A|$.

to a cam mechanism on a variable-speed gear-box driven by a synchronous electric motor above the tank. A cylinder of 6 mm diameter spanned the tank and could be oscillated with simple harmonic motion normal to its longitudinal axis in any direction.

The motion of neutrally buoyant oil drops formed from a mixture of di-ethyl pthalate and butyl pthalate was observed with a travelling microscope. Initially the cylinder was oscillated in a vertical plane and its amplitude was adjusted so that particle displacements within the wave were typically 0·2 mm, which was large compared with the diameter of the oil drops, about 0·01 mm. The maximum distance from the cylinder at which measurements were taken was 0·2 m and, therefore, small compared with the stratification height β^{-1}, which was 7·8 m. Consequently, the experimental results will be compared with the solution of the Boussinesq equations.

Particle movements were measured at a position 60 mm vertically below the cylinder. Particle amplitudes at various frequencies near to the natural frequency are shown in figure 4. The cylinder frequency was adjusted to coincide with the maximum displacement. Displacement profiles were then measured at various x' positions and were found to be similar in shape to those predicted by the analysis close to the x' axis. However, the amplitude did not continue to decrease away from the axis and secondary peaks were consistently found either side of the central peak. These could be due to (*a*) an incorrect forcing frequency, (*b*) variations of the Brunt–Väisälä frequency with altitude or (*c*) reflexions from the top and bottom of the tank. The forcing frequency was then changed, but this merely reduced the amplitudes within the wave; the secondary peaks remained and, therefore, were not due to (*a*). If the Brunt–Väisälä frequency of the fluid increased with distance from the cylinder then an internal wave initially propagating vertically would tend to become inclined away from the vertical,

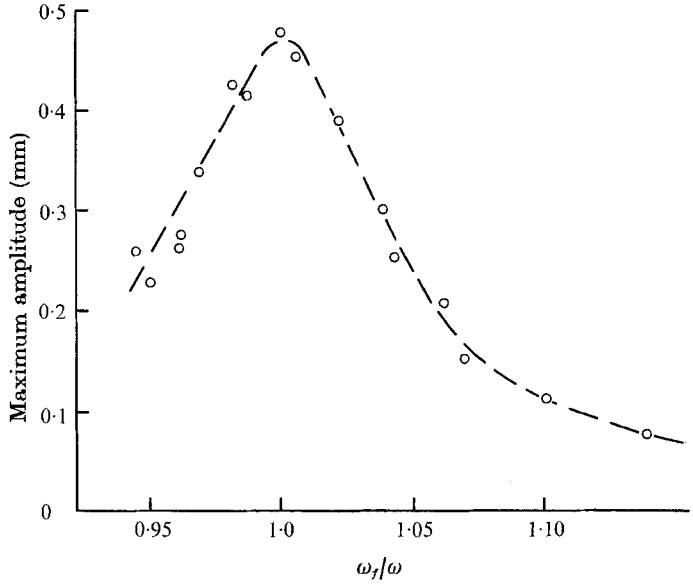

FIGURE 4. Variation of particle amplitude with forcing frequency ω_f at $x' = -60$ mm, $y' = 0$.

as would the particle paths. The cylinder was repositioned so that an internal wave propagating in the opposite direction through the same portion of fluid could be observed. The cylinder frequency was adjusted as before and found to be the same as before but the displacement profiles still had the secondary peaks. If the Brunt–Väisälä frequency in the fluid had varied with height, then a different cylinder frequency would have been obtained and the displacement profiles would have had different properties because they would have been propagating into a fluid with a natural frequency varying in the opposite sense to that previously. As neither of these effects were present and as the particle paths remained in a vertical plane, (*b*) was not the answer.

If the cylinder oscillated in the horizontal plane the amplitudes in the internal waves were very small and difficult to measure except when the amplitude of oscillation of the cylinder was large, in which case there was considerable turbulent mixing around the cylinder. Consequently, all detailed measurements were made with the cylinder oscillating in a vertical plane; the velocities along the x' axis above and below the cylinder were in phase with the cylinder. The analysis will now be extended to include reflexions from the top and bottom of the tank for this case.

We assume that the body is midway between rigid horizontal reflecting surfaces distance h apart. The flow field is approximated by an image system designed to give zero u velocity at the reflecting surfaces. The body and its images lie in a vertical plane and the distance between them is h. The phase difference between consecutive images is π and the nth image above the body has the same phase as the nth image below the body, and if n is even, the phase is that of the body. X is the distance measured vertically upwards from the horizontal level of the

mean position of the body and x_0 is the distance between the mean position and the virtual origin, the point from which the wave appears to originate.

The linear solution to the Boussinesq equations, equation (24), is applied to each image and the contributions are summed. For $0 \leqslant X \leqslant \frac{1}{2}h$ the velocity is

$$u = |A| \left\{ \sum_{n=0}^{\infty} 2(-1)^n \xi \exp(-y^2\xi^2) \cos(y^2\xi^2 - t) + \sum_{n=1}^{\infty} 2(-1)^n \zeta \exp(-y^2\zeta^2) \cos(y^2\zeta^2 - t) \right\}$$

and for $-\frac{1}{2}h \leqslant X \leqslant 0$, $u(X,y,t) = u(-X,y,t)$, where $\xi = \frac{1}{2}(nh + x_0 + X)^{-\frac{1}{2}}$ and $\zeta = \frac{1}{2}(nh + x_0 - X)^{-\frac{1}{2}}$.

By expanding the cosine terms in this expression the velocity may be written as

$$u = |A| (E^2 + G^2)^{\frac{1}{2}} \cos(\tan^{-1}(G/E) - t) \tag{28}$$

and the particle displacement as

$$d = -|A| (E^2 + G^2)^{\frac{1}{2}} \sin(\tan^{-1}(G/E) - t), \tag{29}$$

where $E = B + D$, $G = C + H$ and

$$B = \sum_{n=0}^{\infty} 2(-1)^n \xi \exp(-y^2\xi^2) \cos(y^2\xi^2),$$

$$C = \sum_{n=0}^{\infty} 2(-1)^n \xi \exp(-y^2\xi^2) \sin(y^2\xi^2),$$

$$D = \sum_{n=1}^{\infty} 2(-1)^n \zeta \exp(-y^2\zeta^2) \cos(y^2\zeta^2)$$

and

$$H = \sum_{n=1}^{\infty} 2(-1)^n \zeta \exp(-y^2\zeta^2) \sin(y^2\zeta^2).$$

The displacement envelope is given by

$$e = |A| (E^2 + G^2)^{\frac{1}{2}} \tag{30}$$

and the phase lag at an antinode, the value of t for which $\partial u/\partial t = 0$, is

$$t_p = \tan^{-1}(G/E) \pm N\pi. \tag{31}$$

The small, finite, v velocity at the reflecting surfaces will of course result in some viscous dissipation in the immediate vicinity of the wall, but this is not included in the analysis. In the experiments the cylinder was positioned roughly midway between the diffusion boundaries above the base of the tank and below the free surface, with h' values of 0·7 and 0·4 m. The displacement envelopes evaluated from (30) using $\nu = 1{\cdot}3\,\mathrm{mm^2\,s^{-1}}$ and $h' = 0{\cdot}7$ m show secondary peaks either side of the central peak (see figure 5). Some experimental particle displacements along $y' = 0$ are shown to compare reasonably well with equation (30) in figure 6. All the experimental displacements have been multiplied by a constant amplitude coefficient as the theory will not predict the actual amplitude.

Some theoretical and experimental displacement envelopes are compared in figure 7. The position of the peaks and the width of the waves agree quite well

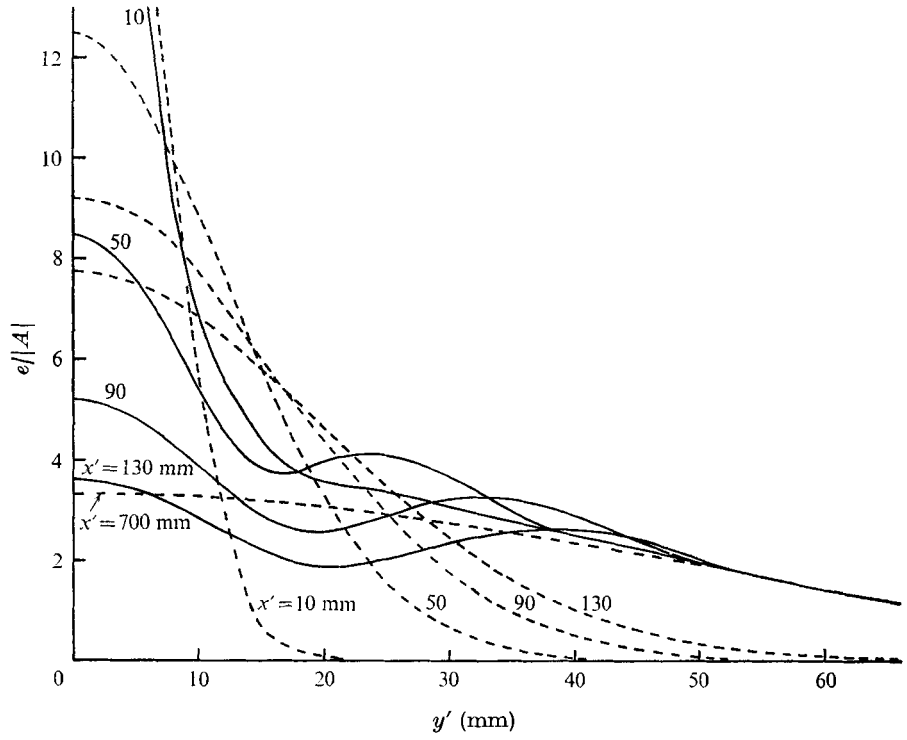

FIGURE 5. The theoretical displacement envelopes at various x' positions. – – –, equation (30) when $h \to \infty$, i.e. with no reflexions; ——, equation (30) when $h' = 0{\cdot}7$ m.

($\nu = 1{\cdot}3$ mm^2 s^{-1}, $\omega = 1{\cdot}12$ rad s^{-1}, $x_0 = 0$.)

but the amplitudes in the secondary peaks do not agree. This is not surprising in view of the simplified theoretical model used to describe the reflecting diffusion boundaries. The waves are obviously very sensitive to small changes in the forcing frequency. This is evident from figure 4 and also from figure 8 (plate 2), which shows schlieren photographs of the internal waves with forcing frequencies close to the natural frequency. The detailed measurements were within 0·5 % of the natural frequency.

Thomas & Stevenson (1972) used a schlieren system to measure the phase velocities in the internal cross-waves. It would be difficult to use this method for the vertically propagating wave because the phase velocity changes so much across the wave. The phase has been measured with a Disa quartz-coated fibre probe, 3 mm in length and 70 μm in diameter, supported on a 200 mm horizontal arm connected to a vertical strut on a traversing mechanism. The fibre probe was used with a constant-temperature hot-wire anemometer set at a low overheating ratio and the output was fed to an X, Y plotter. The phase of the output relative to the phase of the cylinder is compared with equation (31) in figure 9. Outside the primary wave the measured phase lag is slightly larger than the theoretical value. This may be due to (*a*) waves on the diffusion boundaries, (*b*) the disturbance at the horizontal level of the body, or (*c*) a phase lag introduced through

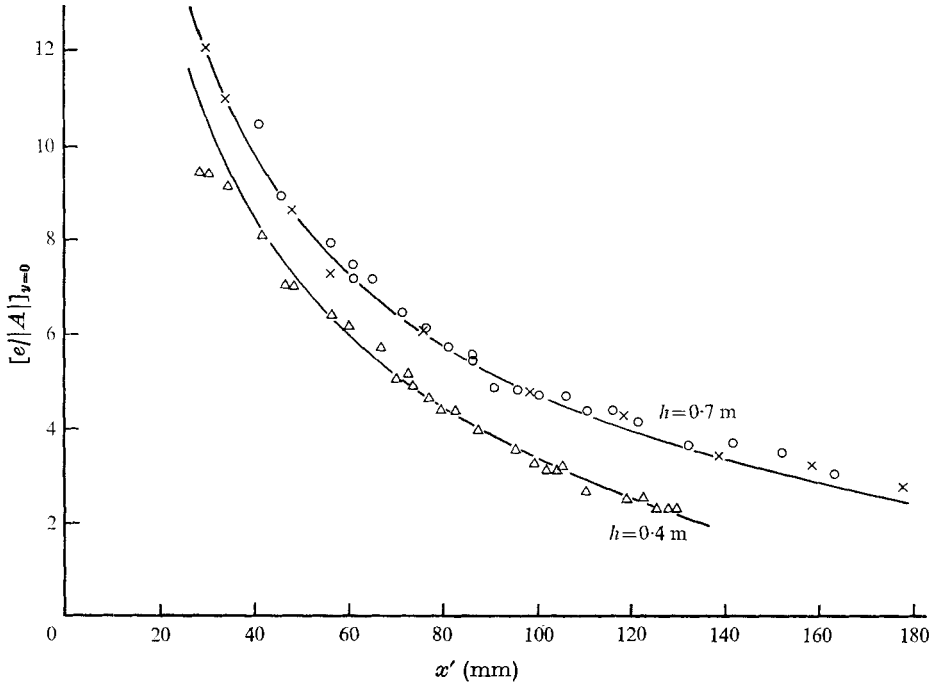

FIGURE 6. The theoretical and experimental variation of the maximum displacements along the centre-line of the wave. ——, theory, equation (30) with $x_0 = 0$. Experimental results: ×, $h' = 0{\cdot}7$ m, $e_M = 0{\cdot}75$ mm; ○, $h' = 0{\cdot}7$ m, $e_M = 0{\cdot}5$ mm; △, $h' = 0{\cdot}4$ m, $e_M = 0{\cdot}12$ mm. e_M is the maximum amplitude at $x' = 0{\cdot}1$ m, $y' = 0$. ($\nu = 1{\cdot}3$ mm^2 s^{-1}, $\omega = 1{\cdot}12$ rad s^{-1}.)

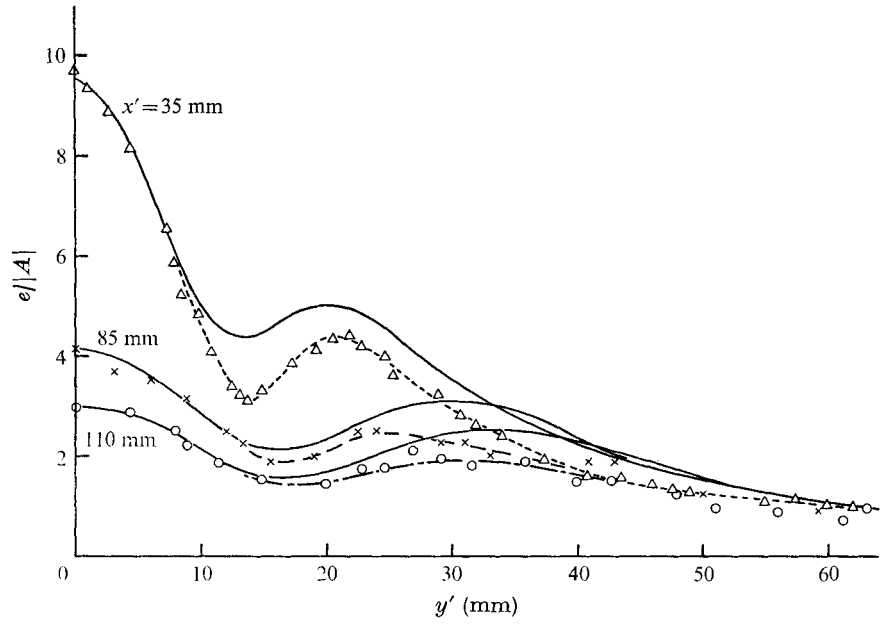

FIGURE 7. Theoretical and experimental displacement envelopes. Experimental results: - - - △ - - -, $x' = 35$ mm; – – × – –, $x' = 85$ mm; ——○——, $x' = 110$ mm. The maximum amplitude at $x' = 0{\cdot}1$ m was 0·12 mm. The unbroken lines are from theory at the same values of x' with $x_0 = 0$. ($h' = 0{\cdot}4$ m, $\nu = 1{\cdot}3$ mm^2 s^{-1}, $\omega = 1{\cdot}12$ rad s^{-1}.)

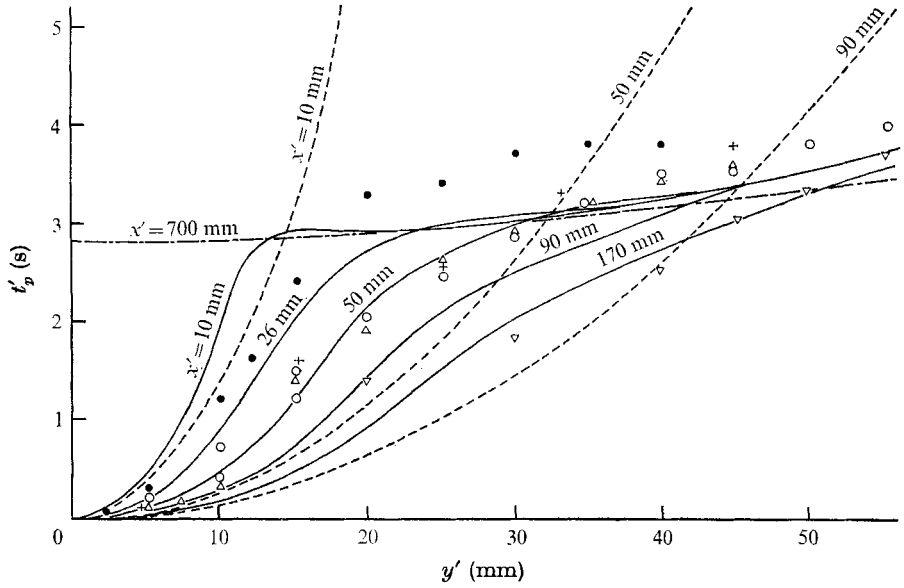

FIGURE 9. The phase lag across the wave at various values of x'. ——, equation (31) when $h = 0{\cdot}7$ m; – – –, equation (31) when $h \to \infty$, i.e. with no reflexions; — · —, with π phase shift. Experimental results: ●, $x' = 26$ mm; △, $x' = 50$ mm; +, $x' = 65$ mm; ○, $x' = 78$ mm; ▽, $x' = 150$ mm. The maximum amplitude at $x' = 0{\cdot}1$ m, $y' = 0$ was 0·5 mm. ($h' = 0{\cdot}7$ m, $\nu = 1{\cdot}3$ mm^2 s^{-1}, $\omega = 1{\cdot}12$ rad s^{-1}.)

the small convection region around the probe. However, the theory with the reflexions certainly accounts qualitatively for the flow in the secondary peaks.

In the theory it was assumed that $a \ll \alpha^2 \ll 1$. In the experiments α^2 was 2×10^{-4} and the resulting condition on a implies that the particle amplitudes must be very much less than 1·5 mm. The conditions were satisfied by the set of results corresponding to an amplitude of 0·12 mm at the 0·1 m position but in the other experiments the amplitudes, although less than 1·5 mm, were rather large.

4. Conclusions

A vertically propagating internal wave corresponding to natural frequency oscillations has been generated and the main features have been described by a small amplitude similarity analysis. The centre-line velocity attenuates as (distance from the forcing region)$^{-\frac{1}{2}}$ and is, therefore, less than in the internal cross-wave, which attenuates as (distance)$^{-\frac{2}{3}}$.

Acknowledgement is made to the Ministry of Defence, who supported this work. D. Gordon was in receipt of a Science Research Council Maintenance Grant.

REFERENCES

GÖRTLER, H. 1943 *Z. angew. Math. Mech.* **23**, 65.
MOWBRAY, D. E. & RARITY, B. S. H. 1967 *J. Fluid Mech.* **28**, 1.
THOMAS, N. H. & STEVENSON, T. N. 1972 *J. Fluid Mech.* **54**, 495.

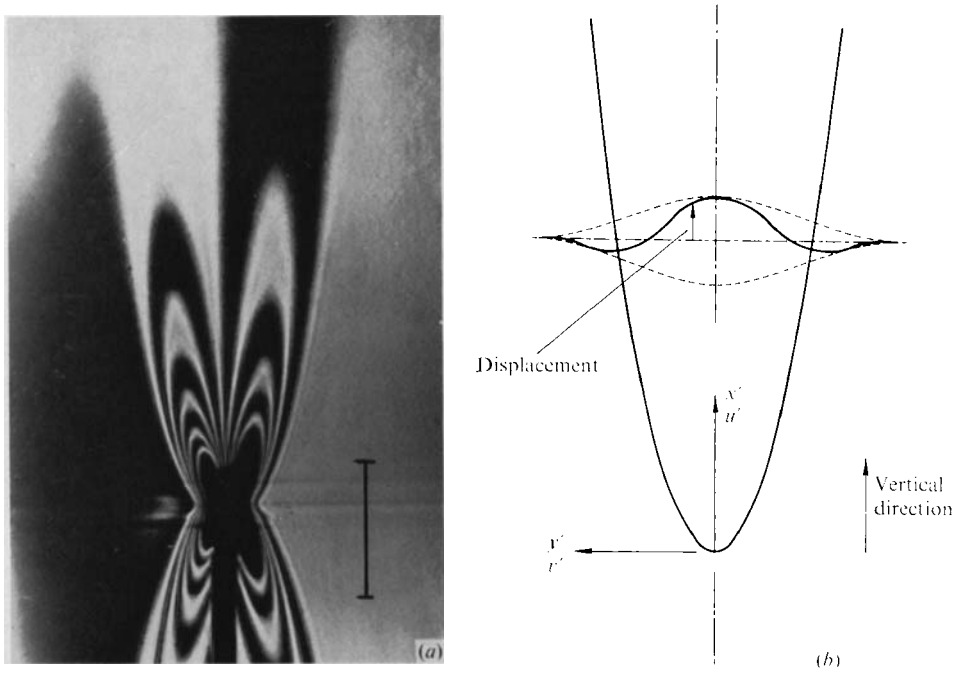

FIGURE 1. (*a*) A schlieren photograph of the internal wave using a vertical grating instead of the usual schlieren knife edge. The scale length is 50 mm. (*b*) The co-ordinate system.

$\omega_f/\omega = 0{\cdot}99$

$\omega_f/\omega = 1{\cdot}00$

$\omega_f/\omega = 1{\cdot}01$

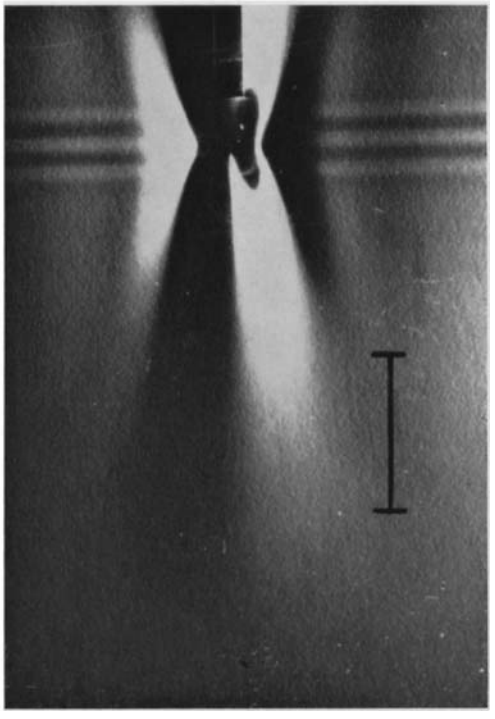

$\omega_f/\omega = 1{\cdot}02$

FIGURE 8. Schlieren photographs of the internal waves at several values of the forcing frequency ω_f close to and at the natural frequency. The only difference between the photographs is the forcing frequency; all the optics are unchanged. A vertical knife edge was used. The scale length is 50 mm.